Enhanced energy storage density by inducing defect dipoles in lead free relaxor ferroelectric $BaTiO_3$-based ceramics

Wen-Bo Li, Di Zhou, and Li-Xia Pang

Articles you may be interested in

Enhanced energy storage density by inducing defect dipoles in lead free relaxor ferroelectric BaTiO$_3$-based ceramics

Wen-Bo Li,[1] Di Zhou,[1,2,a)] and Li-Xia Pang[3]

[1]*Electronic Materials Research Laboratory, Key Laboratory of the Ministry of Education and International Center for Dielectric Research, Xi'an Jiaotong University, Xi'an 710049, Shaanxi, China*
[2]*Department of Materials Science and Engineering, University of Sheffield, S1 3JD Sheffield, United Kingdom*
[3]*Micro-optoelectronic Systems Laboratories, Xi'an Technological University, Xi'an 710032, Shaanxi, China*

In this work, Mn-doped 0.9BaTiO$_3$-0.1Bi(Mg$_{2/3}$Nb$_{1/3}$)O$_3$ ceramics were prepared by the conventional solid state reaction method, and the effect of defect dipoles on energy storage properties of lead free relaxor ferroelectric BaTiO$_3$-based ceramics was studied. The crystal structure, dielectric properties, and energy storage properties were explored in detail. It was found that polarization hysteresis (P-E) loops of 0.9BaTiO$_3$-0.1Bi(Mg$_{2/3}$Nb$_{1/3}$)O$_3$-x wt. % MnCO$_3$ (0.2–0.5) ceramics took on high maximum polarization (P_{max}) and low remanent polarization (P_r). Meanwhile, recoverable energy density (W_{rec}) and energy conversion efficiency (η) were obviously enhanced by inducing defect dipoles into BaTiO$_3$-Bi(Mg$_{2/3}$Nb$_{1/3}$)O$_3$ relaxor ferroelectrics. The 0.9BaTiO$_3$-0.1Bi(Mg$_{2/3}$Nb$_{1/3}$)O$_3$-0.3 wt. % MnCO$_3$ ceramic was found to exhibit good energy storage properties with a W_{rec} of about 1.70 J/cm^3 and a $\eta \sim 90\%$ under an electric field of 210 kV/cm. The breakdown electric field and W_{rec} of BaTiO$_3$-based materials were significantly increased in the present work, and they might be good candidates for high power energy storage applications. *Published by AIP Publishing.* [http://dx.doi.org/10.1063/1.4979467]

The search for materials with high dielectric breakdown strength and discharged energy density for high power capacitors has been widely explored recently. Nowadays, energy storage capacitors with the capability of ultra-fast charging-discharging ($<1 \mu$s) are widely used in modern electronics and electrical power systems.[1–6] For a dielectric capacitor, high maximum polarization (P$_{max}$), low remnant polarization (P$_r$), and the breakdown electric field (BDS) are desired for achieving high recoverable energy density (W$_{rec}$) and energy conversion efficiency (η). In general, three kinds of ceramic materials are used in capacitors: linear dielectrics, anti-ferroelectric (AFE), and ferroelectric (FE). For linear dielectrics,

$$W = \frac{1}{2}DE = \frac{1}{2}\varepsilon_r\varepsilon_0 E^2, \qquad (1)$$

where ε_r is the dielectric constant of the ceramic and ε_0 is the vacuum permittivity. As for AFE and FE ceramics,

$$W = \int EdP, \qquad (2)$$

where E is the applied-field and P is the polarization. The dielectric constant of AFE and FE ceramics is larger than that of the linear dielectrics. So, they are promising for higher energy density than linear dielectrics. The low BDS and W$_{rec}$ of AFE and FE ceramics limit their application for high-voltage equipment and compact electronic devices.[7–10] So, it is important to search for the materials with a high BDS and W$_{rec}$ to enable the increasing demands for more compact electronic and energy storage devices.

In recent years, many efforts have been focused on improving the energy storage properties of AFE and FE. According to Equation (2), the energy density of AFE and FE ceramics can be determined from the area between the vertical axes and the electric displacement-electric field discharge curve. So, there are two possible routes to improve the energy-storage density of AFE and FE ceramics for energy storage applications: One is to enhance the BDS for high E and another is to increase the limit of integration by enlarging the difference between the P_{max} and P_r. For the first route, it was found that AFE ceramic (Pb$_{0.88}$La$_{0.08}$)(Zr$_{0.91}$Ti$_{0.09}$)O$_3$ by the conventional solid-state sintering process has good energy storage properties with a W_{rec} of 3.04 J/cm^3 and a η of 92% under an applied electric field of 170 kV/cm.[11] Then, AFE ceramics (Pb$_{0.97}$–xSr$_x$La$_{0.02}$)(Zr$_{0.75}$Sn$_{0.195}$Ti$_{0.055}$)O$_3$ have a higher energy density (W_{rec} = 5.56 J/cm^3 under 350 kV/cm).[12] Compared with other PZT based materials, (Pb$_{0.88}$La$_{0.08}$)(Zr$_{0.91}$Ti$_{0.09}$)O$_3$ ceramics exhibit a much higher E$_A$, E$_F$, and BSD. In order to enhance the energy storage properties of BaTiO$_3$-based FE ceramics, some oxides with extra high BDS are used as additives to enhance the BDS, such as Al$_2$O$_3$, SiO$_2$, MgO, and so on.[13–15] For example, BaTiO$_3$ ceramics by coating powders with Al$_2$O$_3$ and SiO$_2$ with an enhanced energy storage density of 0.725 J/cm^3 with $\eta \sim 80\%$ had been prepared by Liu et al.[13] Zhang et al.[14] reported that the BST-MgO composite possesses the W_{rec} of about 1.14 J/cm^3. Huang et al.[15] obtained the BST-MgO composite by spark plasma sintering with the W_{rec} of about 1.5 J/cm^3 and $\eta \sim 88.5\%$ and so on. While previous work mainly focused on increasing the BDS values to obtain larger energy storage density, less attention was paid on the technique of enlarging the difference between P_{max} and P_r values. A recent study showed that

a)Author to whom correspondence should be addressed. Electronic mail: zhoudi1220@gmail.com. Tel./Fax: +86-29-82668679.

relaxor ferroelectrics exhibit a high energy density with a large difference between P_{max} and P_r values, for example, 0.7BaTiO₃-0.3BiScO₃ single dielectric layer capacitors with a high energy density of 6.1 J/cm at 730 kV/cm.[16] Then, a series of relaxor ferroelectrics BaTiO₃-Bi(M₂/₃Nb₁/₃)O₃ and BaTiO₃-Bi(M₁/₂Ti₁/₂)O₃ (M = Mg and Zn) ceramics were studied, and the energy storage densities of relaxor ferroelectrics were around from 1 to 2 J/cm³.[17–21] It indicated that partial occupancy of Bi³⁺ at the A site of the perovskite compound could effectively improve the energy storage properties. As a promising candidate system, relaxor ferroelectrics BaTiO₃ (BT)-based ceramics play a key role in the area of energy density capacitors because of their low P_{max}, high P_r, and low loss. It is well-known that the defect dipole has a great impact on the functional properties of ferroelectrics. The study found that the defect dipole can create a defect dipole moment (P_D), which can act as an internal field to switch the new domain back to its original state when an electric field is removed. In order to further increase the difference between P_{max} and P_r values, defect dipoles are induced into ferroelectrics. Recently, some researchers found that Mn²⁺ was doped into TiO₂, and KNbO₃ can form defect dipoles. As an acceptor dopant, the addition of Mn²⁺ may generate oxygen vacancies ($V_{\ddot{O}}$). It strongly affects the phase transition, ceramic density, and dielectric losses.[22–25] Cao et al. reported that the TiO₂ ceramics with the concentration of about 0.05 mol. % Manganese doped possessed good dielectric properties with low loss tangent, high BDS, and energy storage density.[22] Rafiq et al. studied the defects and charge transport in Mn-doped K₀.₅Na₀.₅NbO₃ ceramics and clarify the effect of Mn²⁺ on the electrical properties of KNN ceramics when doped at the B-site.[23] However, the Mn²⁺ effect on the energy storage properties of BT ceramics has not yet been systematically addressed. In the present work, the 0.9BaTiO₃-0.1Bi(Mg₂/₃Nb₁/₃)O₃-x wt. % MnCO₃ (0.2–0.5) ceramics were reported. We studied the effect of Mn²⁺ doping on sintering behavior, microstructures, and energy storage properties of 0.9BaTiO₃-0.1Bi(Mg₂/₃Nb₁/₃)O₃ ceramics.

Proportionate amounts of reagent-grade BaCO₃ (99.84%), rutile TiO₂(>99.84%), Bi₂O₃(99%), MgO (98%,), Nb₂O₅ (99.5%), and MnCO₃ (98%) as the starting reactants were used. The 0.9BaTiO₃-0.1Bi(Mg₂/₃Nb₁/₃)O₃-x wt. % MnCO₃ (x = 0.2, 0.3, 0.4, and 0.5) ceramics were synthesized by the conventional solid state reaction method. Crystalline structures were investigated by using X-ray diffraction (XRD) with Cu Kα radiation (Rigaku D/MAX-2400 X-ray diffractometer, Tokyo, Japan). Microstructures were observed on fractured surfaces with a scanning electron microscope (SEM) (SEM; Quanta 250F, FEI). To determine the dielectric properties, the sintered samples were polished and coated with silver on both surfaces. The temperature dependence of the dielectric constant and loss was determined at a frequency of 1 MHz by means of a LCR meter (HP 4980, Agilent, Palo Alto, CA) interfaced with a computer, where the specimens were heated at a rate of 2 °C/min from 25 °C to 400 °C. The BDS of the samples was determined at an ambient temperature using a high voltage source (HF5013 K; Huiyou Electronics Co. Ltd., Chang Zhou, China). At least 10 specimens were used for the BDS testing.

Polarization–electric field (P–E) hysteresis loops were measured at room temperature by using a TF Analyzer 2000 (aix ACCT) ferroelectric test system. The electric field was applied from 1 to 220 kV/cm with a triangular wave form under 10 Hz during measurement.

Fig. 1 exhibits the XRD patterns of the 0.9BaTiO₃-0.1Bi(Mg₂/₃Nb₁/₃)O₃-x wt. % MnCO₃ (x = 0.2, 0.3, 0.4, 0.5) ceramics sintered at their optimal temperatures. It is seen that all the samples exhibited the perovskite structure without any appreciable secondary impurity phases, indicating that Mn ions can diffuse into the 0.9BaTiO₃-0.1Bi(Mg₂/₃Nb₁/₃)O₃ lattices to form a solid solution. All the peaks were well indexed according to the standard diffraction peaks (PDF #34-0411).

Fig. 2 shows the temperature dependence of dielectric constant (ε_r) and dielectric loss (tan δ) of the 0.9BaTiO₃-0.1Bi(Mg₂/₃Nb₁/₃)O₃-x wt. % MnCO₃ (x = 0.2, 0.3, 0.4, and 0.5) ceramics in the temperature range of 25 °C to 400 °C. The ε_r-T and tan δ-T curves were measured at 1 MHz. From Fig. 2, it can be seen that ε_r of the Mn-doped 0.9BaTiO₃-0.1Bi (Mg₂/₃Nb₁/₃)O₃ decreased, while tan δ increased as the temperature increased. Previous studies reported that Mn²⁺ doping had been used in systems to mitigate the sintering temperature and dielectric losses.[24–26] With the content of Mn²⁺, ε_r of samples did not change significantly, while tan δ keeps quite low at room temperature in this work. The ε_r and tan δ values of the 0.9BaTiO₃-0.1Bi(Mg₂/₃Nb₁/₃)O₃-x wt. % MnCO₃ composite ceramics were 1180–1280 and <0.001, respectively. It indicated that Mn doping in 0.9BaTiO₃-0.1Bi(Mg₂/₃Nb₁/₃)O₃ could mitigate dielectric losses significantly.

In order to obtain the value of energy storage density, the Weibull distribution of the BDS for Mn-doped 0.9BaTiO3-0.1Bi(Mg₂/₃Nb₁/₃)O₃ ceramics is shown in Fig. 3(a). The Weibull distribution can be described by the following equations:

$$X_i = \ln(E_i), \quad (3)$$

$$Y_i = \ln\left(-\ln\left(1 - \frac{i}{1 + n}\right)\right), \quad (4)$$

where X_i and Y_i are the two parameters in the Weibull distribution function, E_i is the specific breakdown voltage of each
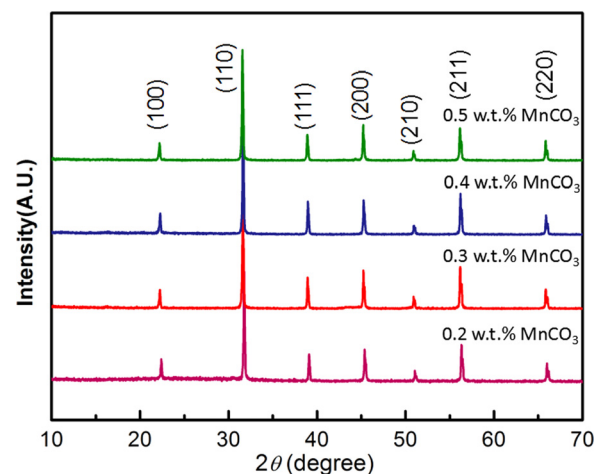

FIG. 1. XRD patterns of 0.9BaTiO₃-0.1Bi(Mg₂/₃Nb₁/₃)O₃-x wt. % MnCO₃ (0.2 ≤ x ≤ 0.5) ceramics.
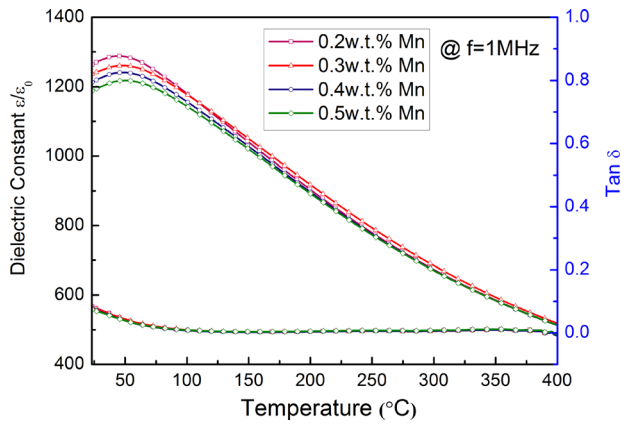
FIG. 2. Temperature dependence of the dielectric constant and loss of $0.9BaTiO_3$-$0.1Bi(Mg_{2/3}Nb_{1/3})O_3$-x wt. % $MnCO_3$ ($0.2 \leq x \leq 0.5$) ceramics measured in the temperature range of $25\,^\circ C$ to $400\,^\circ C$.

specimen in the experiments, n is the sum of specimens of each sample, and i is the rank of specimens. From Fig. 3(a), X_i and Y_i have a linear relationship and all data points fit well with the Weibull distribution and the shape parameters m are larger than 11 for each composition. The BDS of $0.9BaTiO_3$-$0.1Bi(Mg_{2/3}Nb_{1/3})O_3$-x wt. % $MnCO_3$ (x = 0.2, 0.3, 0.4, and 0.5) ceramics is 264 kV/cm, 268 kV/cm, 277 kV/cm, and 274 kV/cm, respectively. As shown in Fig. 3(a), it can be seen that the BDS of the $0.9BaTiO_3$-$0.1Bi(Mg_{2/3}Nb_{1/3})O_3$-x wt. % $MnCO_3$ ceramic is improved with the increase in the Mn^{2+} content. While the content of Mn^{2+} increases further, the BDS decreases and the $0.9BaTiO_3$-$0.1Bi(Mg_{2/3}Nb_{1/3})O_3$-x wt. % $MnCO_3$ ceramic obtains a maximum of 277 kV/cm at x = 0.4. Previous studies showed that the grain size and porosity could affect the BDS in the ceramic.[20] Hence, the higher BDS can be obtained by decreasing grain size and porosity. It indicates that the dense

microstructure and high BDS are achieved in Mn^{2+} doped $0.9BaTiO_3$-$0.1Bi(Mg_{2/3}Nb_{1/3})O_3$ ceramics. The values of BDS are significantly higher than the other BT-based bulk ceramics.

In order to study the influence of the Mn^{2+} content on the P_{max}, P_r, and P_{max}–P_r of ceramics, bipolar polarization–electric field (P–E) hysteresis loops of the $0.9BaTiO_3$-$0.1Bi(Mg_{2/3}Nb_{1/3})O_3$-x wt. % $MnCO_3$ (x = 0.2, 0.3, 0.4, are 0.5) are measured at the same applied electric field 150 kV/cm in Fig. S1 (supplementary material). From Fig. 3(c), the P_{max}-P_r value goes to a maximum and then decreases with the further increase in Mn^{2+} is doped at the same applied electric field and the P_{max}-P_r values of the $0.9BaTiO_3$-$0.1Bi(Mg_{2/3}Nb_{1/3})O_3$-x wt. % $MnCO_3$ (x = 0.2, 0.3, 0.4, and 0.5) are 15.46 $\mu C/cm^2$, 16.28 $\mu C/cm^2$, 16.13 $\mu C/cm^2$, and 15.11 $\mu C/cm^2$, respectively. The result shows that the defect dipoles can lead to an apparent enhancement in polarization simultaneously. Fig. S2 (supplementary material) shows that P-E hysteresis loops of the $0.9BaTiO_3$-$0.1Bi(Mg_{2/3}Nb_{1/3})O_3$-x wt. % $MnCO_3$ (x = 0, 0.2, 0.3, 0.4, and 0.5) ceramics are measured with 10 Hz unipolar triangle signals at their critical BDS. The energy storage properties of the $0.9BaTiO_3$-$0.1Bi(Mg_{2/3}Nb_{1/3})O_3$-x wt. % $MnCO_3$ (x = 0, 0.2, 0.3, 0.4, and 0.5) ceramics are investigated using their bipolar polarization–electric field (P–E) hysteresis loops. As for antiferroelectric and ferroelectric ceramics, it is well known that the energy storage density (W) is determined by the dielectric constant and the breakdown strength[14]

$$W = \int_0^{P_{max}} EdP, \tag{5}$$

$$W_{rec} = \int_{Pr}^{P_{max}} EdP, \tag{6}$$
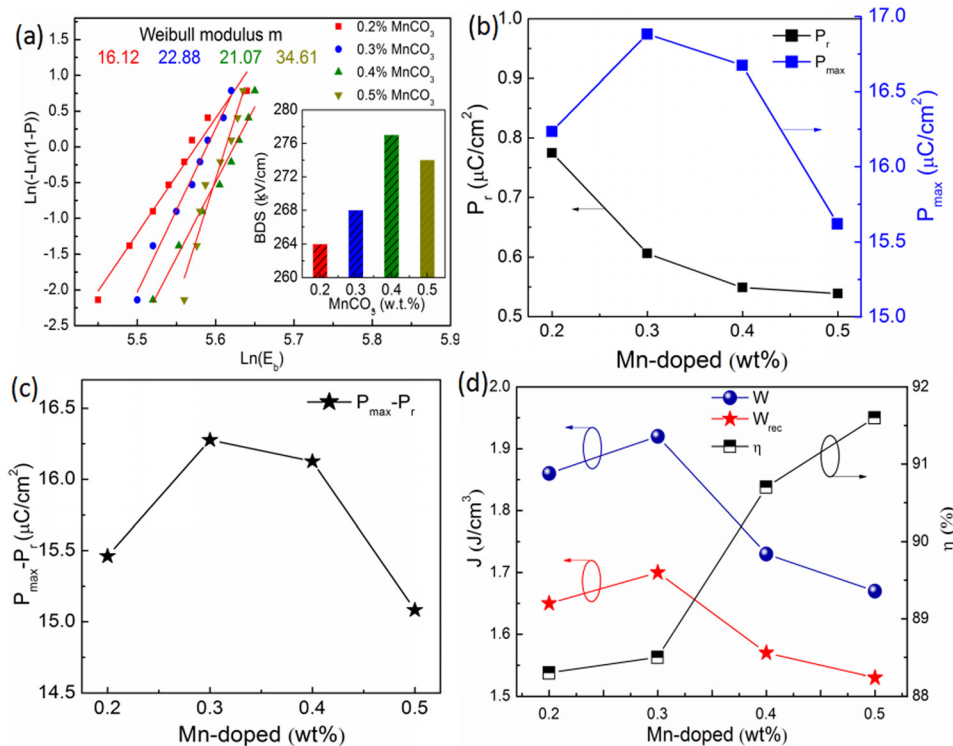
$$\eta = \frac{W_{rec}}{W} \times 100\%, \tag{7}$$

FIG. 3. Weibull distributions and the fitting lines of the BDS (a), P_{max}, P_r (b), and P_{max}-P_r (c) values measured to be the same at the same applied electric field of 150 kV/cm and energy storage density of $0.9BaTiO_3$-$0.1Bi(Mg_{2/3}Nb_{1/3})O_3$-x wt. % $MnCO_3$ ($0.2 \leq x \leq 0.5$) ceramics was measured at their critical BDS (d).

where W, W_{rec}, E, P_r, P_{max}, and η are the charged stored energy density, the discharge stored energy density, the applied electric field, the remnant polarization, the maximum polarization, and the energy storage efficiency, respectively. The charged stored energy density (W), recoverable energy density (W_{rec}), and energy storage efficiency (η) of the $0.9BaTiO_3$-$0.1Bi(Mg_{2/3}Nb_{1/3})O_3$-$x$ wt. % $MnCO_3$ ($x = 0$, 0.2, 0.3, 0.4, and 0.5) ceramics as a function of the content of Mn^{2+} at room temperature are shown in Fig. 3(d) and Table S1 (supplementary material). When the x values increase from 0.2 to 0.5, the W and W_{rec} increase to maximum and then decrease. The variation of W and W_{rec} is similar to P_{max}–P_r. It indicated that Mn-doped $0.9BaTiO_3$-$0.1Bi(Mg_{2/3}Nb_{1/3})O_3$ can effectively enhance W, W_{rec}, and η. The maximum value of W and W_{rec} can be up to $1.92\,J/cm^3$ and $1.7\,J/cm^3$ when 0.3 wt. % is doped, respectively. It can be observed that η increases from 88.2% to 91.6% with the content of Mn^{2+} that increases from 0.2 to 0.5 wt. %. It is found that the optimum energy storage properties of the $0.9BaTiO_3$-$0.1Bi(Mg_{2/3}Nb_{1/3})O_3$-$x$ wt. % $MnCO_3$ ceramics are obtained at $x = 0.3$ with a W_{rec} of about $1.7\,J/cm^3$ and $\eta \sim 88.6\%$ under an electric field $210\,kV/cm$.

Fig. 4(a) shows that the unipolar P-E hysteresis loops of the $0.9BaTiO_3$–$0.1Bi(Mg_{2/3}Nb_{1/3})O_3$–$0.3$ wt. % $MnCO_3$ ceramic are measured at room temperature under different electric fields. As shown in Fig. 4(a), unipolar P-E loops become thick as the electric field increases, which indicated that P_{max}, W, and W_{rec} increased, while the P_r and η decreased. Fig. 4(b) shows the energy storage properties of the $0.9BaTiO_3$-$0.1Bi(Mg_{2/3}Nb_{1/3})O_3$-$0.3$ wt. % $MnCO_3$ ceramic as a function of electric field. It can be observed that W increased from $0.162\,J/cm^3$ to $1.92\,J/cm^3$ as electric fields increased from $50\,kV/cm$ to $210\,kV/cm$ and W_{rec} increased from $0.153\,J/cm^3$ to $1.7\,J/cm^3$. The η decreases with the increasing applied electric field because of the increase in energy loss. For energy storage efficiency, it always kept a high efficiency ($>88.5\%$) when the applied electric field reached $210\,kV/cm$. In this work, the dielectric breakdown strength and discharged energy density values are considerably higher than some other lead-free ceramics, indicating that the $0.9BaTiO_3$-$0.1Bi(Mg_{2/3}Nb_{1/3})O_3$-$x$ wt. % $MnCO_3$ ($x = 0.2$, 0.3, 0.4, and 0.5) ceramics are promising candidates for high power energy storage applications.
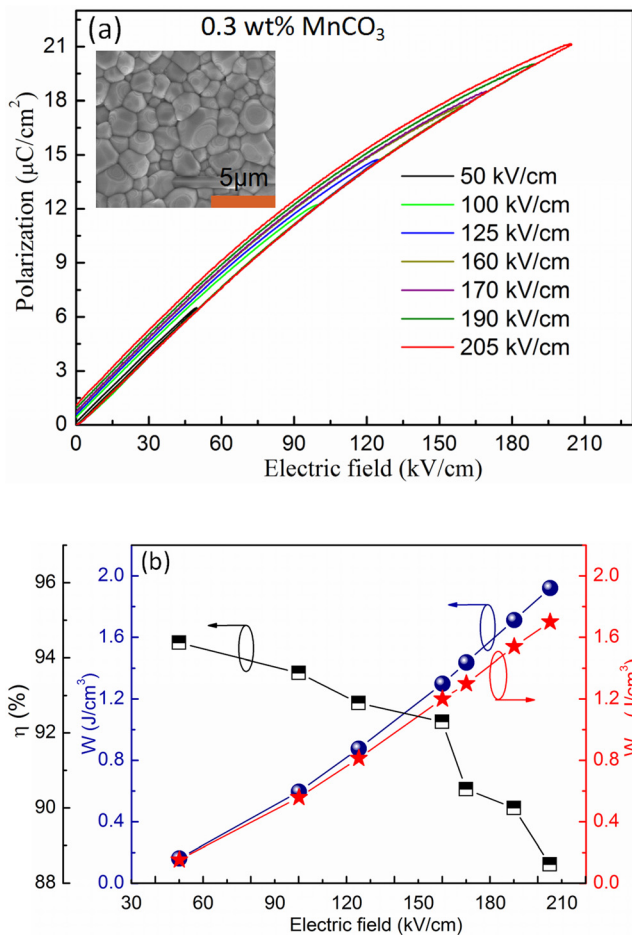
In summary, a series of high dielectric breakdown strength and discharged energy density $0.9BaTiO_3$-$0.1Bi(Mg_{2/3}Nb_{1/3})O_3$-$x$ wt. % $MnCO_3$ ($x = 0.2$, 0.3, 0.4, and 0.5) ceramics were prepared by using the conventional solid state reaction method. All the samples could be well densified at $1180\,°C \sim 1220\,°C$. XRD analysis indicated that $0.9BaTiO_3$–$0.1Bi(Mg_{2/3}Nb_{1/3})O_3$-$x$ wt. % $MnCO_3$ ($x = 0.2$, 0.3, 0.4, and 0.5) exhibited the perovskite structure. High P_{max} and P_{max}–P_r can be achieved by introducing defect dipoles. As a result, $0.9BaTiO_3$-$0.1Bi(Mg_{2/3}Nb_{1/3})O_3$-$x$ wt. % $MnCO_3$ ($x = 0.2$, 0.3, 0.4, and 0.5) ceramics exhibited good energy storage properties with high charged stored energy density ($1.92\,J/cm^3$), charged stored energy density ($1.7\,J/cm^3$), and η ($>88.5\%$), which is a promising lead-free material for high density energy storage capacitor applications.

See supplementary material for the measurement scheme of P_{max} and P_r, bipolar P–E hysteresis loops near electric breakdown, and energy storage properties of $0.9BaTiO_3$-$0.1Bi(Mg_{2/3}Nb_{1/3})O_3$-$x$ wt. % $MnCO_3$ ($0.0 \leq x \leq 0.5$) ceramics.

FIG. 4. (a) The unipolar P-E hysteresis of $0.9BaTiO_3$-$0.1Bi(Mg_{2/3}Nb_{1/3})O_3$-$0.3$ wt. % $MnCO_3$ ceramics at room temperatures under different electric fields. (b) The calculated energy storage density W, the recoverable energy storage density W_{rec}, and energy storage efficiency (η %).

[1]G. R. Love, J. Am. Ceram. Soc. **73**, 323 (1990).
[2]I. Burn and D. M. Smyth, J. Mater. Sci. **7**, 339 (1972).
[3]J. J. Xu, Z. L. Wang, D. Xu, F. Z. Meng, and X. B. Zhang, Energy Environ. Sci. **7**, 2213 (2014).
[4]S. Kwon, W. Hackenberger, E. Alberta, E. Furman, and M. Lanagan, IEEE Electr. Insul. Mag. **27**, 43 (2011).
[5]W. B. Hu, Y. Liu, R. L. Withers, T. J. Frankcombe, L. Norén, A. Snashall, M. Kitchin, P. Smith, B. Gong, H. Chen, J. Schiemer, F. Brink, and J. W. Leung, Nat. Mater. **12**, 821 (2013).
[6]Q. Li, G. Zhang, F. Liu, K. Han, M. R. Gadinski, C. Xiong, and Q. Wang, Energy Environ. Sci. **8**, 922 (2015).
[7]J. Kuwata, K. Uchino, and S. Nomura, Ferroelectrics **22**, 863 (1979).

[8]Y. Song, Y. Shen, P. H. Hu, Y. H. Lin, M. Li, and C. W. Nan, Appl. Phys. Lett. **101**, 152904 (2012).

[9]J. L. Pan, K. Li, J. J. Li, T. Hsu, and Q. Wang, Appl. Phys. Lett. **95**, 022902 (2009).

[10]D. P. Shay, N. J. Podraza, N. J. Donnelly, and C. A. Randall, J. Am. Ceram. Soc. **95**, 1348 (2012).

[11]H. R. Jo and C. S. Lynch, J. Appl. Phys. **119**, 024104 (2016).

[12]Q. F. Zhang, H. F. Tong, J. Chen, Y. M. Lu, T. Q. Yang, X. Yao, and Y. B. He, Appl. Phys. Lett. **109**, 262901 (2016).

[13]B. B. Liu, X. H. Wang, Q. C. Zhao, and L. T. Li, J. Am. Ceram. Soc. **98**, 2641 (2015).

[14]Q. M. Zhang, L. Wang, J. Luo, Q. Tang, and J. Du, Int. J. Appl. Ceram. Technol. **7**, E124–E128 (2010).

[15]Y. H. Huang, Y. J. Wu, W. J. Qiu, J. Li, and X. M. Chen, J. Eur. Ceram. Soc. **35**, 1469 (2015).

[16]H. Ogihara, C. A. Randall, and S. Trolier-McKinstry, J. Am. Ceram. Soc. **92**, 1719 (2009).

[17]Z. Liu, X. Chen, W. Peng, C. Xu, X. Dong, F. Cao, and G. Wang, Appl. Phys. Lett. **106**, 262901 (2015).

[18]T. Wang, L. Jin, C. C. Li, Q. Y. Hu, and X. Y. Wei, J. Am. Ceram. Soc. **98**, 559 (2015).

[19]Q. Y. Hu, L. Jin, T. Wang, C. C. Li, Z. Xing, and X. Y. Wei, J. Alloys Compd. **640**, 416 (2015).

[20]Z. B. Shen, X. H. Wang, B. C. Luo, and L. T. Li, J. Mater. Chem. A **3**, 18146 (2015).

[21]L. W. Wu, X. H. Wang, and L. T. Li, RSC Adv. **6**, 14273 (2016).

[22]S. Chao and F. Dogan, J. Am. Ceram. Soc. **94**, 179 (2011).

[23]M. A. Rafiq, A. Tkach, M. E. Costa, and P. M. Vilarinho, Phys. Chem. Chem. Phys. **17**, 24403 (2015).

[24]W. F. Liu, W. Chen, L. Yang, Y. Wang, L. X. Zhang, C. Zhou, S. T. Li, and X. B. Ren, Mater. Sci. Eng. A **438–440**, 350 (2006).

[25]Z. Y. Feng and X. B. Ren, Appl. Phys. Lett. **91**, 032904 (2007).

[26]W. P. Cao, W. L. Li, Y. Feng, T. Bai, Y. L. Qiao, Y. F. Hou, T. D. Zhang, Y. Yu, and W. D. Fei, Appl. Phys. Lett. **108**, 202902 (2016).